Circulation

ORIGINAL RESEARCH ARTICLE

Dicer in Macrophages Prevents Atherosclerosis by Promoting Mitochondrial Oxidative Metabolism

Yuanyuan Wei, PhD
Judit Corbalán-Campos, MSc*
Rashmi Gurung, MD*
Lucia Natarelli, PhD
Mengyu Zhu, PhD
Nicole Exner, PhD
Florian Erhard, PhD
Franziska Greulich, PhD
Claudia Geißler, BSc
N. Henriette Uhlenhaut, PhD
Ralf Zimmer, PhD
Andreas Schober, MD

BACKGROUND: Alternative macrophage activation, which relies on mitochondrial oxidative metabolism, plays a central role in the resolution of inflammation and prevents atherosclerosis. Moreover, macrophages handle large amounts of cholesterol and triglycerides derived from the engulfed modified lipoproteins during atherosclerosis. Although several microRNAs regulate macrophage polarization, the role of the microRNA-generating enzyme Dicer in macrophage activation during atherosclerosis is unknown.

METHODS: To evaluate the role of Dicer in atherosclerosis, *Apoe*$^{-/-}$ mice with or without macrophage-specific *Dicer* deletion were fed a high-fat diet for 12 weeks. Anti-argonaute 2 RNA immunoprecipitation chip and RNA deep sequencing combined with microRNA functional screening were performed in the *Dicer* wild-type and knockout bone marrow–derived macrophages to identify the individual microRNAs and the mRNA targets mediating the phenotypic effects of Dicer. The role of the identified individual microRNA and its target in atherosclerosis was determined by tail vein injection of the target site blockers in atherosclerotic *Apoe*$^{-/-}$ mice.

RESULTS: We show that *Dicer* deletion in macrophages accelerated atherosclerosis in mice, along with enhanced inflammatory response and increased lipid accumulation in lesional macrophages. In vitro, alternative activation was limited whereas lipid-filled foam cell formation was exacerbated in *Dicer*-deficient macrophages as a result of impaired mitochondrial fatty acid oxidative metabolism. Rescue of microRNA (miR)-10a, let-7b, and miR-195a expression restored the oxidative metabolism in alternatively activated *Dicer*-deficient macrophages. Suppression of ligand-dependent nuclear receptor corepressor by miR-10a promoted fatty acid oxidation, which mediated the lipolytic and anti-inflammatory effect of Dicer. miR-10a expression was negatively correlated to the progression of atherosclerosis in humans. Blocking the interaction between ligand-dependent nuclear receptor corepressor and miR-10a by target site blockers aggravated atherosclerosis development in mice.

CONCLUSIONS: Dicer plays an atheroprotective role by coordinately regulating the inflammatory response and lipid metabolism in macrophages through enhancing fatty acid–fueled mitochondrial respiration, suggesting that promoting Dicer/miR-10a–dependent metabolic reprogramming in macrophages has potential therapeutic implications to prevent atherosclerosis.

*Ms Corbalán-Campos and Dr Gurung contributed equally.

Key Words: atherosclerosis ■ foam cells ■ macrophages ■ metabolism ■ microRNAs ■ mitochondria

Sources of Funding, see page 2018

https://www.ahajournals.org/journal/circ

Clinical Perspective

What Is New?

- MicroRNA biogenesis, for example, of the microRNAs miR-10a and let-7b, promotes the degradation of fatty acids by mitochondrial respiration in macrophages, which reduces intracellular lipid storage and limits atherosclerosis.

What Are the Clinical Implications?

- Reducing foam cell formation in atherosclerotic arteries by enhancing energy metabolism through microRNA-mediated fatty acid oxidation may be a promising approach for the treatment of atherosclerosis.

At bifurcations and curvatures of arteries, circulating lipoproteins such as low-density lipoproteins (LDLs) enter the vessel wall through leaky junctions frequently associated with enhanced endothelial cell turnover.[1,2] In the subendothelial space, chemical modifications of LDL result in the unrestricted uptake of these particles by monocyte-derived macrophages through scavenger receptors such as CD36.[3] Surplus lipids that cannot be introduced into the reverse cholesterol transport or degraded by mitochondrial β-oxidation are stored as cholesteryl ester and triglycerides in lipid droplets. Excessive lipid accumulation in lesional macrophages (a process called foam cell formation) is associated with increased oxygen consumption in early atherosclerosis, indicating a role of mitochondria in managing lipid excess by fatty acid oxidation (FAO).[4–6] However, oxygen consumption declines during lesion progression, which may decrease the degradation of triglycerides and thereby promote macrophage apoptosis.[5,7] The high lipid content of dead foam cells in turn poses a metabolic threat to macrophages clearing the vessel wall.[8] Engulfment of apoptotic cells upregulates ATP-binding cassette transporters ABCA1 and ABCG1 by nuclear receptors retinoid X receptor (RXR) heterodimers, which protects the efferocyte from apoptosis as a result of cholesterol overload by increasing cholesterol efflux and increases phagocytosis.[9–11] In advanced atherosclerosis, efferocytosis is defective, leading to the formation of a necrotic core consisting of cell debris and thrombogenic lipids.[12] The necrotic core characterizes vulnerable lesions that are prone to rupture and result in thrombotic obstruction of arteries.[13]

Inflammatory activation of macrophages by Toll-like receptor 4 agonists such as lipopolysaccharide results in intracellular lipid storage and foam cell formation by activating the transcription factor hypoxia-inducible factor-1α, which shifts energy metabolism from FAO and oxidative phosphorylation (OXPHOS) to glycolysis.[4,14–16] Instead of producing ATP, mitochondria in lipopolysaccharide-stimulated macrophages primarily generate reactive oxygen species, which promote their proinflammatory state and antimicrobial activity.[17,18] Moreover, oxygen is used to produce nitric oxide after lipopolysaccharide-induced upregulation of nitric oxide synthase 2.[19,20] By replacing oxidative energy production, glycolytic ATP synthesis protects inflammatory macrophages from cell death.[21] In contrast, alternative macrophage activation by interleukin-4 (IL-4) limits lipid droplet formation; increases oxygen consumption, FAO, and OXPHOS; and promotes an anti-inflammatory phenotype.[22] IL-4 induces the transcription of genes involved in FAO and mitochondrial biogenesis through STAT6-mediated upregulation of peroxisome proliferator-activated receptor (PPAR)-γ coactivator (PGC)-1β,[23,24] which is a transcriptional coactivator of PPARα and nuclear respiratory factor 1.[24] In addition, sirtuin1 (Sirt1) activates PGC-1β by deacetylation and promotes FAO in macrophages during inflammation resolution.[25,26] The increased OXPHOS in alternatively activated macrophages (AAMs) is associated with prolonged survival, downregulation of nitric oxide synthase 2, and improved phagocytosis.[22,27]

MicroRNAs (miRNAs) regulate macrophage activation by promoting (eg, miR-155) or inhibiting (eg, miR-223) inflammatory signaling pathways.[28,29] Moreover, miRNAs play key roles in macrophage cholesterol metabolism, for instance, through suppression of cholesterol efflux by targeting ABCA1, and are involved in foam cell formation.[28] In atherosclerosis, upregulation of miR-155 in foam cells enhances necrotic core formation by inhibiting efferocytosis.[30] The endoribonuclease Dicer produces 21- to 25-nucleotide-long RNA duplexes by cleaving the terminal loop of precursor miRNAs and transfers the duplexes to Argonaut proteins in the RNA-induced silencing complexes, which are activated by removal of one of the strands of the RNA duplexes.[31] Because of the short seed sequence of 6 to 7 nucleotides, miRNAs usually bind to hundreds of target mRNAs, and conversely, 1 mRNA transcript can be targeted by multiple miRNAs.[32] It is notable that global miRNA expression is substantially decreased in macrophages from cigarette smokers as a result of inhibition of Dicer by SUOMylation.[33] In mice, *Dicer* knockout increases inflammatory activation of tumor-associated macrophages,[34] suggesting that Dicer may play a role in macrophage polarization. However, the concerted effect of the miRNA network in macrophages on atherosclerosis is still incompletely understood.

In the present study, we identified Dicer as a positive regulator of FAO and OXPHOS in macrophages, which promoted an AAM phenotype and limited foam cell formation. In mice, *Dicer* knockout in macrophages fostered atherosclerosis characterized by enhanced inflammation, foam cell formation, macrophage apoptosis, and necrot-

ic core formation in the lesions. Dicer generated miRNAs such as miR-10a and let-7b, which increased mitochondrial respiration by targeting corepressors of nuclear receptors such as ligand-dependent nuclear receptor corepressor (Lcor). Blocking the interaction between miR-10a and Lcor aggravated atherosclerosis progression in mice. Therefore, Dicer and miRNAs (eg, miR-10a) integrate the immune system and lipid metabolism by promoting FAO and OXPHOS during macrophage activation through inhibiting the corepressors of nuclear receptors, which prevents atherosclerosis.

METHODS

Data Disclosure Statement

The data that support the findings of this study are available from the corresponding author on reasonable request.

Animal Models

To generate *Apoe*$^{-/-}$ mice containing a loxP site-flanked *Dicer* sequence[35] and a transgene with Cre recombinase under the control of the myeloid cell–specific M-lysozyme (LysM) promoter, *LysM*^{Cre} mice were crossed with *Dicer*$^{flox/flox}$/*Apoe*$^{-/-}$ mice (The Jackson Laboratory) to obtain *LysM*^{Cre}/*Dicer*$^{WT/flox}$/*Apoe*$^{-/-}$ mice. *LysM*^{Cre}/*Dicer*$^{flox/flox}$/*Apoe*$^{-/-}$ (*M-Dicer*$^{-/-}$) and *LysM*^{Cre}/*Dicer*$^{WT/WT}$/*Apoe*$^{-/-}$ (*M-Dicer*$^{+/+}$) littermates (6–8 weeks old) were fed a high-fat diet (HFD) comprising 21% crude fat (E15721-347, Ssniff) for 12 weeks. The aortas and aortic roots were harvested after in situ perfusion with 4% paraformaldehyde (Carl Roth), PAXgene (Qiagen), or RNAlater (Thermo Fisher Scientific) via the left ventricle. All animal experiments were reviewed and approved by the local authorities (State Agency for Nature, Environment and Consumer Protection of North Rhein-Westphalia and District Government of Upper Bavaria) in accordance with the German animal protection laws.

Transfection

Lipofectamine RNAiMAX Reagent (Thermo Fisher Scientific) was used to transfect murine bone marrow–derived macrophages (BMDMs) with mirVana miRNA mimics (30 nmol/L; Thermo Fisher Scientific), LNA-modified miRNA inhibitors (50 nmol/L; Exiqon), GapmeRs (50 nmol/L; Exiqon), target site blockers (TSBs; 50 nmol/L; Exiqon), or scrambled controls. The sequences of miRNA inhibitors, GapmeRs, and TSBs are listed in Table I in the online-only Data Supplement.

Anti-Argonaute 2 RNA Immunoprecipitation Chip (AGO2-RIP-Chip)

The AGO2-RIP of *Dicer*$^{+/+}$ or *Dicer*$^{-/-}$ BMDMs was performed as described previously.[29] Input RNA and AGO2- or immunoglobulin G (IgG)–immunoprecipitated (IP) RNA were reverse transcribed and preamplified with Ovation PicoSL WTA System V2 (NuGEN) followed by the microarray analysis. Agilent SurePrint G3 Mouse Gene Expression microarrays (8×60 K format, Agilent Technologies) were used in combination with a 1-color–based hybridization protocol (IMGM Laboratories GmbH). Raw signals on the microarrays were scanned with the Agilent DNA Microarray Scanner (Agilent Technologies).

To quantify the gene enrichment in AGO2 complexes, RIP-chip data were analyzed according to a method described previously.[36] Probe intensity values were estimated with Feature Extraction 10.7.3.1 software (Agilent Technologies). All arrays were quantile normalized. Enrichment values were computed for AGO2-IP against input, AGO2-IP against IgG-IP, and IgG-IP against input (for our results, we used the enrichment of AGO2-IP against IgG-IP). To account for differing pulldown efficiencies, a second normalization was performed on enrichment values using principal component analysis. Significantly enriched genes were determined with a normal mixture modeling approach to distinguish nonassociated mRNAs from mRNAs enriched in AGO2 complexes. Because the background distribution of intensity values from Agilent arrays is different from Affymetrix arrays used in previously,[36] the normal mixture models were only estimated by using probes flagged as "IsWellAboveBG." With the use of TargetScan 6.2 algorithms, the miRNA target sites were predicted in those mRNAs that were upregulated (cutoff, 2-fold) but less enriched at least by 50% in AGO2 complexes of *Dicer*$^{-/-}$ BMDMs compared with *Dicer*$^{+/+}$ BMDMs.

RNA-Sequencing

Total RNA was extracted from resting *Dicer*$^{+/+}$ or *Dicer*$^{-/-}$ BMDMs with the RNeasy Mini Kit (Qiagen) with on-column DNase digest. We used 500 ng RNA as input to the TruSeq mRNA library preparation kit (RS-122–2103, Illumina) and sequenced on the Illumina HiSeq3000. FastQC (http://www.bioinformatics.babraham.ac.uk/projects/fastqc/) was performed for quality control. The reads were mapped to the mouse genome GRCm38.81 (mm10), and reads overlapping genes were counted simultaneously with STAR aligner version 2.4.1d[37] with the following options: –outFilterMultimapNmax 20 –alignSJoverhangMin 8 – alignSJDBoverhangMin 1 –outFilterMismatchNmax 999 –outFilterMismatchNoverLmax 0.04 –alignIntronMin 20 –alignIntronMax 1000000 –alignMatesGapMax 100000 –quantMode GeneCounts. DeSeq2[38] was used to identify differentially expressed genes in *Dicer*$^{+/+}$ and *Dicer*$^{-/-}$ BMDMs. In brief, Deseq2 uses negative linearized binomial modeling to estimate the dispersion and therefore models differential expression in a data-driven way. Genes showing a mean expression of 50 counts were treated as expressed and when changed 1.5-fold (false discovery rate <0.05) were called differentially expressed. The pathway enrichment (absolute *z* score >2; $P<0.05$) of the differentially expressed mRNAs was investigated by Ingenuity Pathway Analysis (Qiagen). The significance values for the pathways were calculated by 1-sided Fisher exact test.

Quantitative Real-Time Polymerase Chain Reaction

Total RNA was reverse-transcribed with a high-capacity cDNA reverse transcription kit or TaqMan MicroRNA Reverse Transcription Kit (Thermo Fisher Scientific). The mRNA quantitative real-time polymerase chain reaction (PCR) assay was performed with gene-specific primers (Table II in the online-only Data Supplement) and GoTaq qPCR Master Mix (Promega). The miRNA quantitative real-time PCR was performed with TaqMan MicroRNA Assays (Thermo Fisher Scientific). The data were normalized to a single or multiple

reference genes (b2m, Gapdh, and Tbp for mRNA; U6 and sno135 for miRNA), scaled to the sample with the lowest expression (qbase software, Biogazelle), and logarithmically transformed (log10).

Human Carotid Lesion Samples

Human atherosclerotic lesion specimens were obtained from 23 patients (mean age, 75±8 years; 55% were symptomatic; 35% female and 65% male) during endarterectomy. One half of each sample was immediately stored in RNAlater for RNA isolation, and the other half was fixed in paraformaldehyde followed by paraffin embedding and sectioning. The sections were stained with Movat pentachrome staining, and the necrotic core areas were quantified with ImageJ. The Ethics Committee of the Medical Faculty at RWTH Aachen University approved the study protocol for the collection of human atherosclerotic plaque samples, and written informed consent was obtained from all participating subjects.

In Vivo TSB Treatment

After 8 weeks of HFD feeding, male *Apoe*$^{-/-}$ mice (6–8 weeks old) were randomized to the different experimental groups and injected once weekly via the tail vein with miR10a/*Lcor* or control TSBs (20 mg/kg, Exiqon) for 4 weeks. During the injection period, mice were fed a HFD. The tissues were harvested 1 week after the last injection.

Statistical Analysis

Two groups were compared by the unpaired Student *t* test, and >2 groups were compared by 1-way or 2-way ANOVA, depending on the number of grouping variables (Prism, GraphPad Software). For post hoc multiple comparisons after ANOVA, the Tukey-Kramer test was used to compare every mean with every other mean, and unprotected Fisher least significant difference test was performed for planned comparisons without correction. Data from the human plaque samples were analyzed with Pearson correlation coefficient. Values of $P<0.05$ were considered statistically significant.

Data Availability

The RNA sequencing, AGO2-RIP-chip, and miRNA quantitative PCR array data have been deposited in the National Center for Biotechnology Information Gene Expression Omnibus (http://www.ncbi.nlm.nih.gov/geo/) and are accessible with Gene Expression Omnibus series accession number GSE87721 (AGO2-RIP-chip and miRNA quantitative PCR array) and GSE106854 (RNA sequencing).

RESULTS

Dicer Deletion in Macrophages Leads to Enhanced Atherosclerosis in *Apoe*$^{-/-}$ Mice

To investigate the role of macrophage Dicer in atherosclerosis, we generated *Apoe*-deficient mice with a myeloid cell–specific knockout of *Dicer* (*LysM*^{Cre}/*Dicer*$^{flox/flox}$/*Apoe*$^{-/-}$; *M-Dicer*$^{-/-}$ in brief). The null allele was confirmed in BMDMs from *M-Dicer*$^{-/-}$ mice compared with BMDMs from *LysM*^{Cre}/*Dicer*$^{wt/wt}$/*Apoe*$^{-/-}$ (*M-Dicer*$^{+/+}$) mice (Figure IA in the online-only Data Supplement). In *M-Dicer*$^{-/-}$ mice, *Dicer* mRNA expression was reduced by 94% in BMDMs and by 81% in aortic lesions after 12 weeks of HFD feeding (Figure IB and IC in the online-only Data Supplement). *M-Dicer*$^{-/-}$ mice developed more severe atherosclerosis in aortas and aortic roots and larger necrotic core areas in the lesions than *M-Dicer*$^{+/+}$ mice (Figure 1A and 1B and Table III in the online-only Data Supplement). Although lesional macrophage and smooth muscle cell contents were not changed (Figure ID and IE in the online-only Data Supplement), more lesional macrophages accumulated lipid droplets and were apoptotic in *M-Dicer*$^{-/-}$ mice than in *M-Dicer*$^{+/+}$ mice, as shown by perilipin-2 and caspase-3 immunostaining, respectively (Figure 1C and 1D and Figure IF in the online-only Data Supplement). *Dicer* knockout in macrophages increased *Nos2*, *Il1b*, and *Ccl2* expression and reduced *Fizz1* and *Ym1* expression in aortic arch lesions obtained by laser capture microdissection (Figure 1E). However, circulating cholesterol levels and leukocyte counts in *Apoe*$^{-/-}$ mice were not changed by *Dicer* ablation in macrophages (Table III in the online-only Data Supplement). Taken together, our data indicate that macrophage Dicer prevents atherosclerosis by decreasing inflammation, lipid accumulation, and apoptosis of lesional macrophages.

Dicer Promotes Alternative Macrophage Activation Through Metabolic Reprogramming

Next, we studied the effect of Dicer on macrophage polarization. In resting, IL-4–, and lipopolysaccharide/interferon-γ (IFN-γ)–stimulated BMDMs, *Dicer* deficiency increased *Il1b* and *Ccl2* expression levels and downregulated the AAM marker *Mrc1* (Figure 2A). However, opposite to the effect in lipopolysaccharide/IFN-γ–treated macrophages, *Dicer* knockout upregulated *Nos2* and *Tnf* expression and downregulated the expression of the AAM markers *Fizz1* and *Ym1*, in resting and IL-4–treated BMDMs (Figure 2A). It is notable that these data indicate that *Dicer* knockout in resting macrophages and AAMs mimics the proinflammatory effect of *Dicer* deletion on lesional macrophages. To analyze the effect of *Dicer* knockout on signaling pathways, we performed RNA deep sequencing in resting *Dicer*$^{+/+}$ and *Dicer*$^{-/-}$ BMDMs. Pathway analysis of the 826 downregulated genes and the 910 upregulated genes (1.5-fold change cutoff; $P<0.05$; Table IV in the online-only Data Supplement) by Ingenuity Pathway Analysis software showed that nuclear factor-κB, pattern recognition receptor, interferon, and death receptor signaling pathways were activated in *Dicer*$^{-/-}$

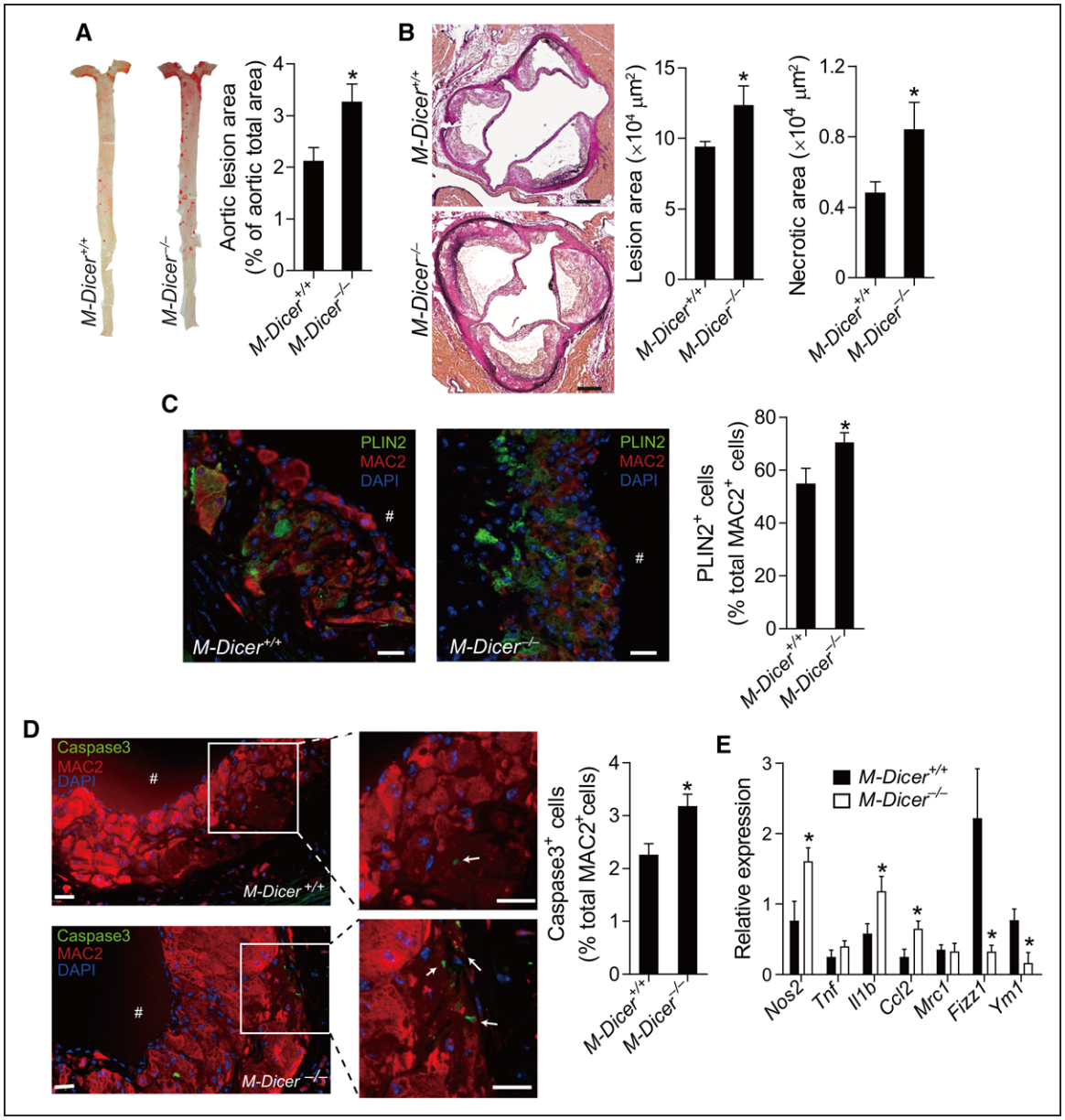

Figure 1. *Dicer* deficiency exacerbates atherosclerosis in *Apoe*$^{-/-}$ mice.
M-Dicer$^{+/+}$ or *M-Dicer*$^{-/-}$ mice were fed the high-fat diet (HFD) for 12 weeks. **A**, Lesion formation in Oil Red O–stained, *en face*–prepared aortas. n=13 or 14 mice per group. **B**, Lesion formation and necrotic core area in aortic roots quantified in sections stained with Elastic van Gieson stain. Scale bars, 200 μm. n=8 or 9 mice per group. **C**, Percentage of lipid droplets containing (perilipin-2 [PLIN2^{+}]–positive) macrophages in lesional macrophages quantified by double immunostaining of PLIN2 (green) and MAC2 (red) in aortic roots. Scale bars, 20 μm. n=8 mice per group. #Lumen. **D**, Percentage of macrophages undergoing cell death (caspase-3^{+}) within the lesion quantified by double immunostaining of cleaved caspase-3 (green) and MAC2 (red) in aortic roots. Arrows indicate the caspase-3^{+} macrophages. Scale bars, 20 μm. n=8 mice per group. #Lumen. **E**, Transcript levels of inflammatory mediators and alternatively activated macrophage markers in atherosclerotic lesions collected via laser capture microdissection from the aortic arch. n=4 to 6 mice per group. All data are presented as mean±SEM. *P<0.05 by Student t test.

BMDMs (Figure 2B). Moreover, PPARα/RXRα signaling was inhibited in *Dicer*$^{-/-}$ BMDMs (Figure 2B), indicating that Dicer affects mitochondrial energy metabolism in macrophages.

IL-4 stimulation increased basal respiration and the maximal respiratory capacity of BMDMs (Figure IIA in the online-only Data Supplement), but it did not affect the extracellular acidification rate compared with vehicle or lipopolysaccharide/IFN-γ treatment (Figure IIB in the online-only Data Supplement). In contrast, lipopolysaccharide/IFN-γ decreased the oxygen consumption rate (OCR) and enhanced the extracellular acidification rate (Figure IIA and IIB in the online-only Data Supplement). Knockout of *Dicer* prevented the stimulatory effect of IL-4 on macrophage respiration and slightly reduced the OCR in resting BMDMs (Figure 2C). However, *Dicer* knockout did not alter the OCR in lipopolysaccharide/IFN-γ–treated BMDMs (Figure 2C). In addition, deletion of *Dicer* did not affect the extracellular acidification rate in resting, IL-4–, or

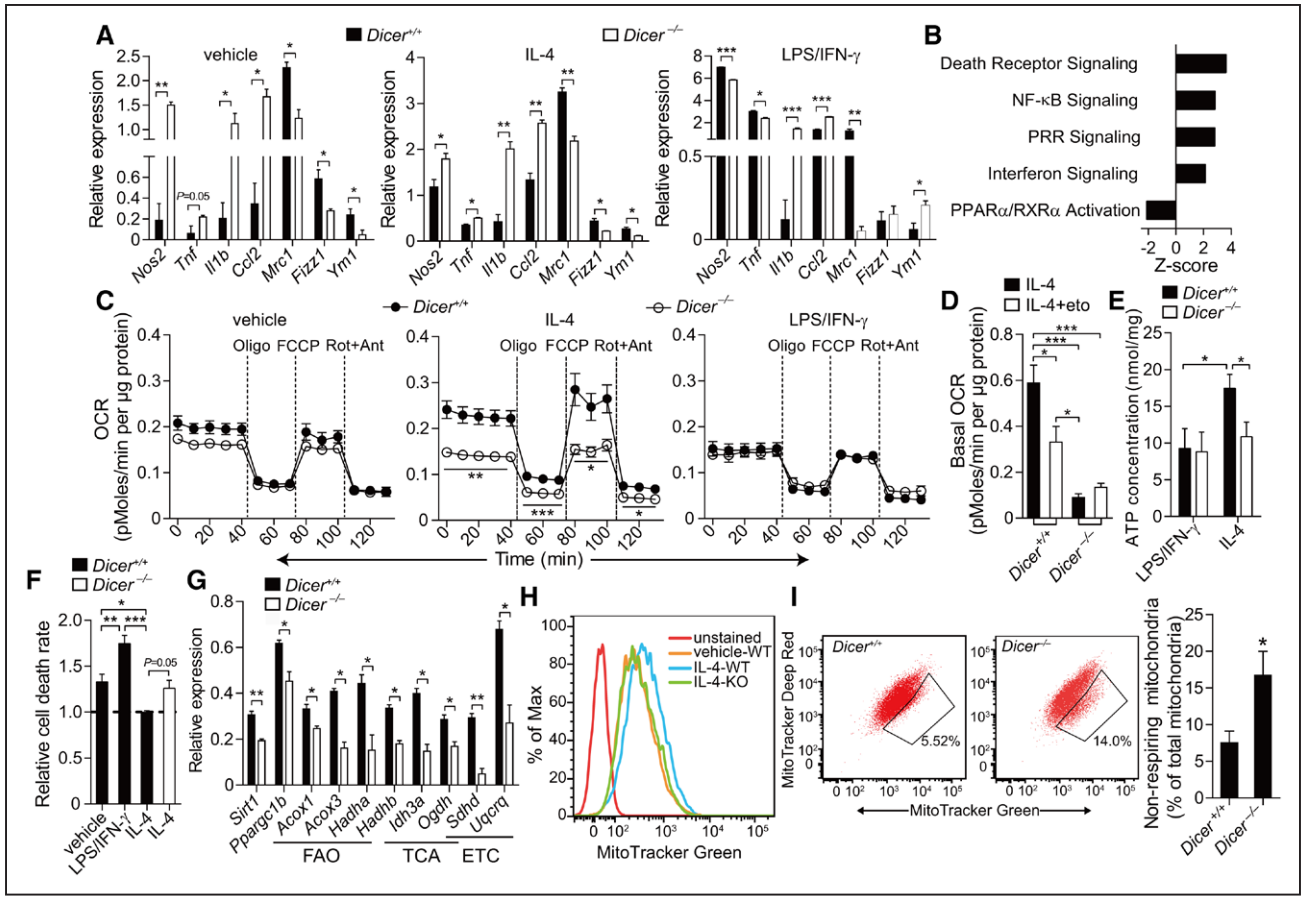

Figure 2. Dicer promotes alternative macrophage activation by enhancing mitochondrial oxidative metabolism.
A, Relative mRNA levels of proinflammatory mediators and alternatively activated macrophage (AAM) markers in *Dicer*$^{+/+}$ and *Dicer*$^{-/-}$ bone marrow–derived macrophages (BMDMs) treated as indicated. n=3. **B**, Downregulated and top 4 upregulated ingenuity canonical pathways (absolute *z* score >2; *P*<0.05) in resting *Dicer*$^{-/-}$ BMDMs compared with *Dicer*$^{+/+}$ BMDMs. n=3. **C**, Oxygen consumption rate (OCR) of vehicle-, interleukin (IL)-4–, or lipopolysaccharide (LPS)/interferon- γ (IFN-γ)–stimulated *Dicer*$^{+/+}$ and *Dicer*$^{-/-}$ BMDMs at the basal condition and after the sequential treatment with oligomycin (Oligo), FCCP, and rotenone/antimycin (Rot+Ant). n=3 or 5. **D** through **F**, Basal OCR (**D**), ATP production (**E**), and relative cell death rate (**F**) in *Dicer*$^{+/+}$ and *Dicer*$^{-/-}$ BMDMs treated as indicated. n=3 to 5. The data in **F** are normalized to the IL-4–treated *Dicer*$^{+/+}$ group. **G**, Relative mRNA levels of genes related to mitochondrial oxidative metabolism in IL-4–stimulated *Dicer*$^{+/+}$ and *Dicer*$^{-/-}$ BMDMs. n=3. **H**, Histograms of flow cytometric analysis of MitoTracker Green staining in *Dicer*$^{+/+}$ (wild-type [WT]) or *Dicer*$^{-/-}$ (knockout [KO]) BMDMs with or without IL-4 treatment. **I**, Contour plots of flow cytometric analysis of double staining with MitoTracker Green and MitoTracker Deep Red in IL-4–treated *Dicer*$^{+/+}$ or *Dicer*$^{-/-}$ BMDMs. n=5. The data in **A**, **C** through **G**, and **I** are presented as mean±SEM. ETC indicates electron transport chain; eto, etomoxir; FAO, fatty acid oxidation; NF-κB, nuclear factor-κB; PPARα, peroxisome proliferator-activated receptor-α; PRR, pattern recognition receptor; RXRα, retinoid X receptor-α; and TCA, tricarboxylic acid cycle. **P*<0.05, ***P*<0.005, and ****P*<0.001 by Student *t* test (**A**, **C**, **G**, and **I**), 1-way ANOVA followed by the Fisher least significant difference test (**F**), and 2-way ANOVA followed by the Tukey-Kramer test (**D** and **E**).

lipopolysaccharide/IFN-γ–treated macrophages (Figure IIB in the online-only Data Supplement). Similar to the effect of *Dicer* knockout, blocking FAO by etomoxir (an inhibitor of carnitine palmitoyltransferase I) inhibited basal respiration in IL-4–stimulated BMDMs (Figure 2D). In IL-4–treated *Dicer*$^{-/-}$ BMDMs, however, etomoxir did not alter the basal OCR (Figure 2D), indicating that FAO contributes to Dicer-mediated respiration in AAMs. Moreover, an increase in ATP production in IL-4–treated compared with lipopolysaccharide/IFN-γ–treated BMDMs was absent in *Dicer*$^{-/-}$ BMDMs (Figure 2E), and *Dicer* knockout abolished the prosurvival effect of IL-4 on macrophages (Figure 2F). In contrast to lipopolysaccharide/IFN-γ, IL-4 increased the expression of genes that enhance mitochondrial function (eg, *Ppargc1b*, the gene name of PGC-1β), FAO (eg, *Hadhb*), and OXPHOS (eg, *Idh3a*; Figure IIC in the online-only Data Supplement). *Dicer* knockout decreased the expression of genes related to mitochondrial function such as *Ppargc1b* and *Sirt1*, FAO, and OXPHOS (Figure 2G). In addition, mitochondrial mass (Figure 2H), mitochondrial DNA content (Figure IID in the online-only Data Supplement), and the number of respiring mitochondria (Figure 2I) were reduced in IL-4–treated *Dicer*$^{-/-}$ BMDMs compared with *Dicer*$^{+/+}$ BMDMs. These data demonstrate that Dicer plays an essential role in alternative macrophage polarization by promoting mitochondrial respiration.

Dicer-Induced Oxidative Metabolism Limits Foam Cell Formation

AAMs are characterized by less lipid droplet formation and increased lipolysis of LDL-derived triglycerides com-

pared with inflammatory macrophages.[22] Hence, we aimed to study the effect of Dicer on foam cell formation. Treatment with oxidized LDL (oxLDL) for 72 hours, which results in foam cell formation, increased basal respiration and the maximal respiratory capacity in BMDMs compared with native LDL and vehicle treatment (Figure 3A). In contrast, oxLDL treatment for 24 or 48 hours did not affect the OCR (Figure III in the online-only Data Supplement), indicating that only excessive lipid accumulation increases mitochondrial respiration. Moreover, oxLDL upregulated *Sirt1*, *Ppargc1b*, *Acox3*, *Hadha/b*, *Uqcrq*, and *Tnf* expression and downregulated *Ym1* expression compared with native LDL (Figure 3B and 3C).

Dicer knockout limited oxLDL-induced mitochondrial respiration (Figure 3D) and upregulation of *Sirt1*, *Ppargc1b*, *Acox3*, *Hadhb*, and *Uqcrq* expression (Figure 3E) but increased lipid accumulation (Figure 3F) in BMDM-derived foam cells. *Fizz1* expression was reduced in *Dicer*$^{-/-}$ BMDMs compared with the wild-type control after oxLDL treatment (Figure 3C). Moreover, blocking the transport of fatty acyl chains into mitochondria with etomoxir decreased the OCR (Figure 3G) and enhanced the lipid accumulation in oxLDL-treated BMDMs (Figure 3F). The effect of etomoxir on foam cell formation was absent in *Dicer*$^{-/-}$ BMDMs (Figure 3F). These findings indicate that excessive lipid accumulation in macrophages is balanced by Dicer-induced oxidative metabolism of fatty acids.

Dicer Drives Macrophage Metabolic Reprogramming by Suppressing Lcor and Nuclear Receptor Corepressor 2

To determine miRNA targets regulated by *Dicer* knockout, we performed miRNA quantitative PCR array and AGO2-RIP-chip analysis in *Dicer*$^{-/-}$ BMDMs and *Dicer*$^{+/+}$ BMDMs. *Dicer* deletion resulted in downregulation of 137 miRNAs, including miRNAs highly expressed in macrophages such as miR-146a, miR-223, let-7 miRNA family members, and miR-142-3p[28] (Figure 4A and Table V in the online-only Data Supplement). Enrichment of AGO2 protein in the AGO2 immunoprecipitate, but not in the IgG immunoprecipitate, was confirmed (Figure IVA in the online-only Data Supplement). We found that 96 mRNAs were both enriched in the RNA-induced silencing complexes of *Dicer*$^{+/+}$ BMDMs compared with that of *Dicer*$^{-/-}$ BMDMs and upregulated by *Dicer* knockout in BMDMs (Table VI in the online-only Data Supplement). Among those 96 genes, 67 mRNAs contained conserved binding

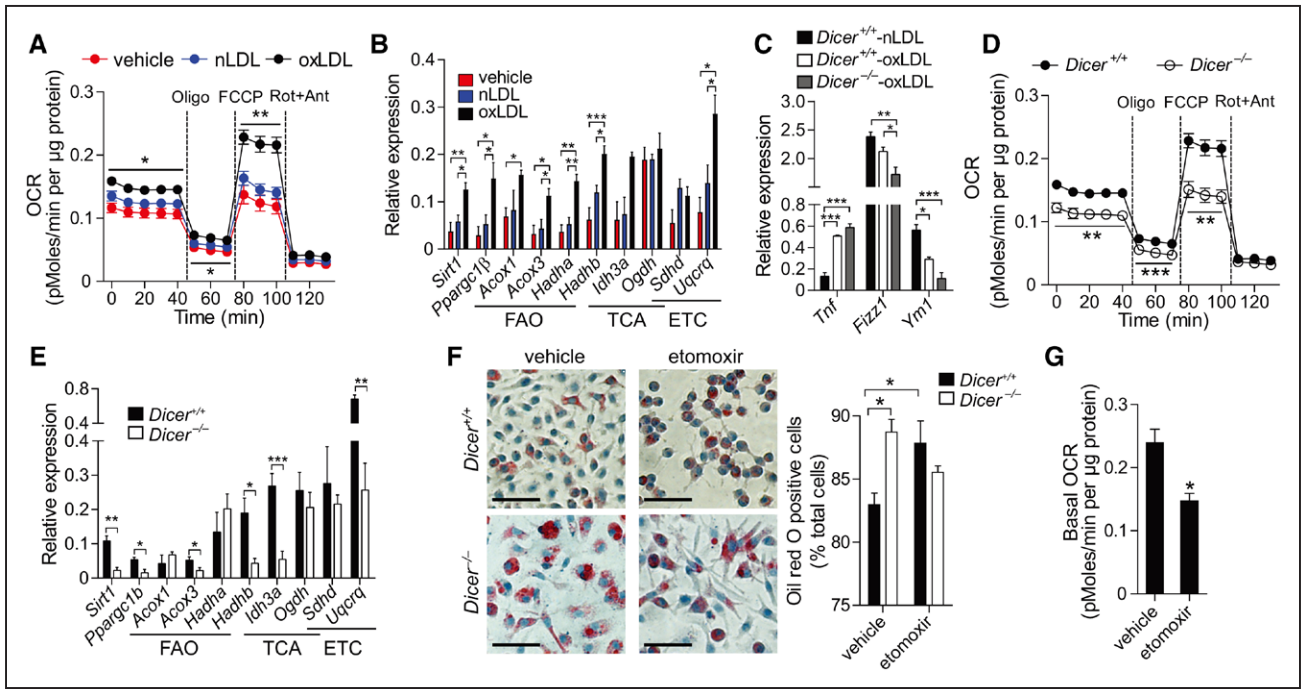

Figure 3. Dicer limits foam cell formation by promoting mitochondrial oxidative metabolism.
Dicer$^{+/+}$ or *Dicer*$^{-/-}$ bone marrow–derived macrophages (BMDMs) were treated with vehicle, native (n) low-density lipoprotein (LDL), or oxidized (ox) LDL for 72 hours. **A**, Oxygen consumption rate (OCR) of vehicle-, nLDL- or oxLDL-treated *Dicer*$^{+/+}$ BMDMs at the basal condition and after the sequential treatment with oligomycin (Oligo), FCCP, and rotenone/antimycin (Rot+Ant). n=5, **P*<0.05 and ***P*<0.005 vs vehicle and nLDL. **B**, Relative mRNA levels of genes related to mitochondrial oxidative metabolism in vehicle-, nLDL-, or oxLDL-treated *Dicer*$^{+/+}$ BMDMs. n=3 or 4. **C**, Relative mRNA levels of *Tnf*, *Fizz1*, and *Ym1* in *Dicer*$^{+/+}$ and *Dicer*$^{-/-}$ BMDMs treated with nLDL or oxLDL. n=3 to 5. **D**, OCR of oxLDL-treated *Dicer*$^{+/+}$ and *Dicer*$^{-/-}$ BMDMs at the basal condition and after the sequential treatment with Oligo, FCCP, and Rot+Ant. n=5. **E**, Relative mRNA levels of genes related to mitochondrial oxidative metabolism in *Dicer*$^{+/+}$ and *Dicer*$^{-/-}$ BMDMs treated with oxLDL. n=4 to 6. **F**, Lipid deposition in oxLDL-treated *Dicer*$^{+/+}$ and *Dicer*$^{-/-}$ BMDMs in the absence or presence of etomoxir determined by Oil Red O staining. Scale bars: 50 µm. n=3 or 4. **G**, Basal OCR of oxLDL-treated *Dicer*$^{+/+}$ BMDMs in the absence or presence of etomoxir. n=4 or 5. All data are presented as mean±SEM. **P*<0.05, ***P*<0.005, and ****P*<0.001 by Student *t* test (**D**, **E**, and **G**), 1-way ANOVA followed by the Fisher least significant difference (**A** and **B**), or Tukey-Kramer (**C**) test and 2-way ANOVA followed by Tukey-Kramer test (**F**). ETC indicates electron transport chain; FAO, fatty acid oxidation; TCA, tricarboxylic acid cycle.

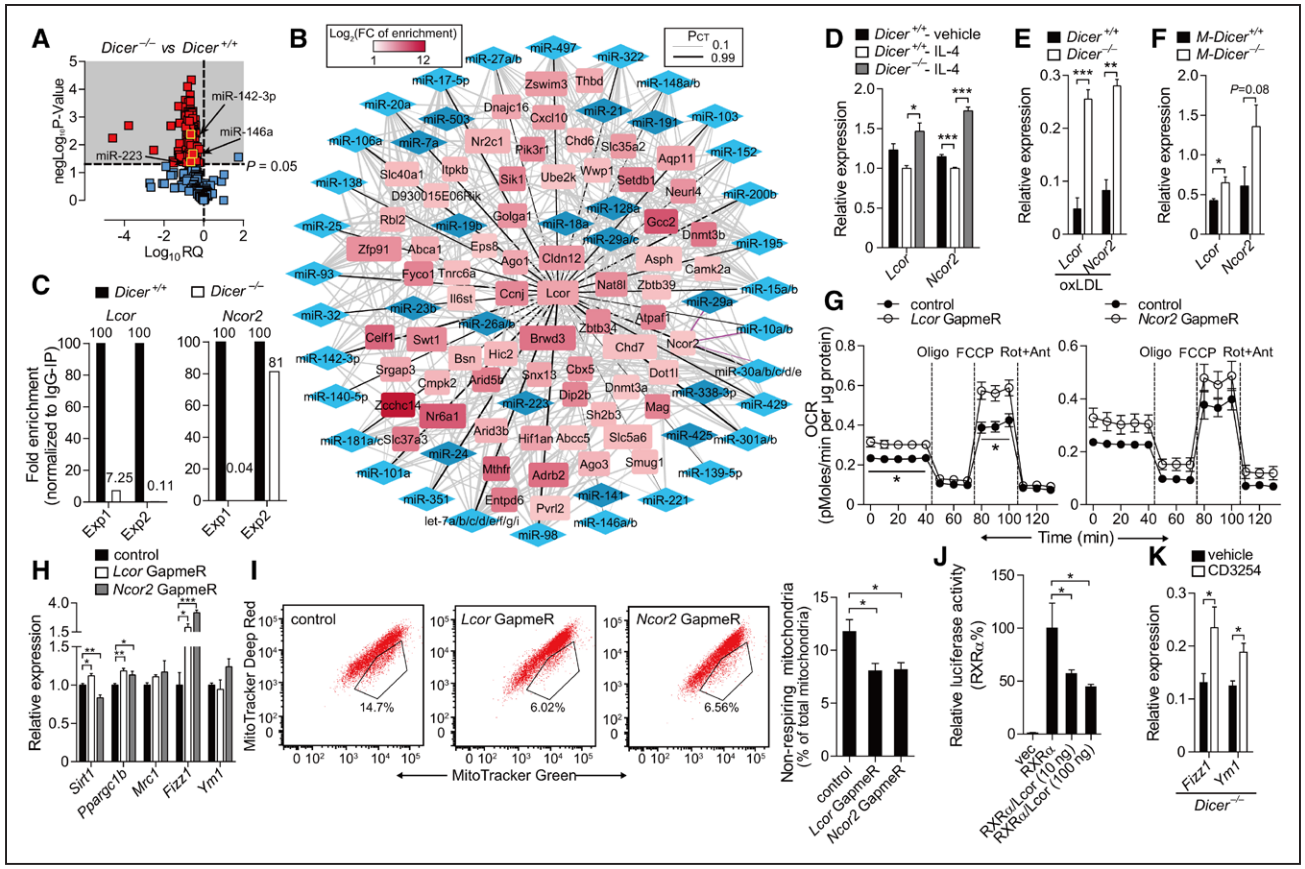

Figure 4. Repressing ligand-dependent nuclear receptor corepressor (Lcor) and nuclear receptor corepressor 2 (Ncor2) mediates Dicer effects on mitochondrial function in alternatively activated macrophages (AAMs).

A, MicroRNA (miRNA) profiles in *Dicer*$^{-/-}$ bone marrow–derived macrophages (BMDMs) compared with *Dicer*$^{+/+}$ BMDMs. Downregulated miRNAs ($P<0.05$) are labeled in red. n=3. **B**, Predicted interactions between downregulated miRNAs and upregulated mRNAs in *Dicer*$^{-/-}$ BMDMs. The rectangle size indicates the fold change (FC; >2) of mRNA expression in *Dicer*$^{-/-}$ vs *Dicer*$^{+/+}$ BMDMs; the rectangle color indicates the FC (>2) of mRNA enrichment in AGO2 complexes of *Dicer*$^{+/+}$ vs *Dicer*$^{-/-}$ BMDMs. miRNAs are shown as diamonds. Light blue diamonds indicate the miRNAs predicted to target Lcor. Black and pink lines indicate Lcor-miRNA and Ncor2-miRNA interactions, respectively. Line thickness represents the probability of conserved targeting (P_{CT}) values that are used to assess biological relevance for predicted miRNA-mRNA interaction by TargetScan. **C**, Enrichment of *Lcor* and *Ncor2* in AGO2-immunoprecipitated RNAs in *Dicer*$^{+/+}$ and *Dicer*$^{-/-}$ BMDMs quantified by quantitative real-time polymerase chain reaction. **D** through **F**, Relative mRNA levels of *Lcor* and *Ncor2* in *Dicer*$^{+/+}$ and *Dicer*$^{-/-}$ BMDMs treated with interleukin-4 (IL-4; **D**; n=3) or oxidized low-density lipoprotein (oxLDL; **E**; n=3 or 5) and in aortic arch lesions of *M-Dicer*$^{+/+}$ and *M-Dicer*$^{-/-}$ mice after 12-week high-fat diet period (**F**; n=4 or 5). **G** through **I**, Oxygen consumption rate (OCR; **G**; n=3 or 4), relative gene expression (**H;** n=4 or 5), and nonrespiring mitochondria ratio (**I;** n=4) in *Dicer*$^{-/-}$ AAMs transfected with *Lcor*, *Ncor2*, or control GapmeRs. **J**, Relative luciferase activity in HEK293T cells cotransfected with reporters containing retinoid X receptor (RXR) transcriptional response elements along with RXRα overexpression, Lcor overexpression, or control (vec) vectors in the presence of 9-cis-retinoic acid. n=3 to 5. **K**, Relative mRNA levels of *Fizz1* and *Ym1* in *Dicer*$^{-/-}$ AAMs treated with or without CD3254. n=3 to 5. The data in **D** through **K** are presented as mean±SEM. **P*<0.05, ***P*<0.005 and ****P*<0.001 by Student *t* test (**E** through **G** and **K**), 1-way ANOVA followed by the Fisher least significant difference (**H** through **J**), or Tukey-Kramer (**D**) test. Oligo indicates oligomycin; and Rot+Ant, rotenone/antimycin.

sites for the miRNAs downregulated in *Dicer*$^{-/-}$ BMDMs as predicted by the TargetScan algorithm (Figure 4B). The highest number of conserved miRNA binding sites (eg, for miR-10a/b, let-7, miR-30, and miR-195) was predicted in the 3′ untranslated region (UTR) of Lcor mRNA (Figure 4B), which encodes for a protein that interacts with RXRα.[39] Binding sites for miR-10 and miR-30 family members were also predicted in the nuclear receptor corepressor 2 (*Ncor2*) mRNA (Figure 4B), which translates into a protein that inhibits PPARα activation and mitochondrial oxidative metabolism.[40] Enrichment of *Lcor* and *Ncor2* in the RNA-induced silencing complexes of *Dicer*$^{+/+}$ compared with *Dicer*$^{-/-}$ BMDMs was confirmed by quantitative real-time PCR (Figure 4C). IL-4 downregulated *Ncor2* and oxLDL downregulated *Lcor* and *Ncor2*, which was prevented by *Dicer* knockout in BMDMs (Figure 4D and 4E and Figure IVB in the online-only Data Supplement). In vivo, *Lcor* and *Ncor2* mRNA levels were higher in atherosclerotic lesions of *M-Dicer*$^{-/-}$ mice than in those from *M-Dicer*$^{+/+}$ mice (Figure 4F). LCoR and NCoR2 were detected mainly in the nucleus of lesional macrophages by immunostaining, and the nuclear localization of LCoR and NcoR2 was more prominent in *M-Dicer*$^{-/-}$ mice than in *M-Dicer*$^{+/+}$ mice (Figure IVC and IVD in the online-only Data Supplement).

To study the role of Lcor and Ncor2 in Dicer-mediated mitochondrial energy metabolism, *Lcor* or *Ncor2* was silenced in IL-4–treated *Dicer*$^{-/-}$ BMDMs by locked nucleic acid–modified GapmeRs. *Lcor* knockdown (Figure V in the online-only Data Supplement) increased basal respira-

tion and maximal respiratory capacity (Figure 4G); upregulated *Sirt1*, *Ppargc1b*, and *Fizz1* expression (Figure 4H); and reduced the number of nonrespiring mitochondria (Figure 4I). *Ncor2* knockdown (Figure V in the online-only Data Supplement) upregulated *Ppargc1b* and *Fizz1* expression (Figure 4H) but reduced the number of nonrespiring mitochondria (Figure 4I). Next we studied the effect of LCoR on the transcriptional activity of RXRα. We transfected HEK293T cells with a vector containing the luciferase gene controlled by RXR transcriptional response elements and a vector expressing RXRα. Overexpression of Lcor inhibited luciferase activity in 9-cis-retinoic acid–treated cells, indicating that LCoR inhibits RXRα activity (Figure 4J). Treatment of IL-4–treated *Dicer*$^{-/-}$ BMDMs with the RXRα agonist CD3254 increased *Fizz1* and *Ym1* expression (Figure 4K). These data indicate that Dicer promotes mitochondrial oxidative metabolism in macrophages by suppressing Lcor and Ncor2.

miR-10a and let-7b Mediate the Effect of Dicer on Macrophage Oxidative Metabolism

To determine the miRNAs that are responsible for the phenotype of *Dicer*$^{-/-}$ macrophages, we studied the role of 13 miRNAs downregulated in *Dicer*$^{-/-}$ macrophages and predicted to target Lcor in the cellular oxygen consumption of AAMs. Transfection of miR-10a, let-7b, or miR-195a mimics increased mitochondrial respiration in IL-4–treated *Dicer*$^{-/-}$ BMDMs (Figure 5A). In contrast, miR-103, let-7a/i, miR-98, or miR-200b mimic treatment did not affect and miR-30a, miR-106b, miR-142,

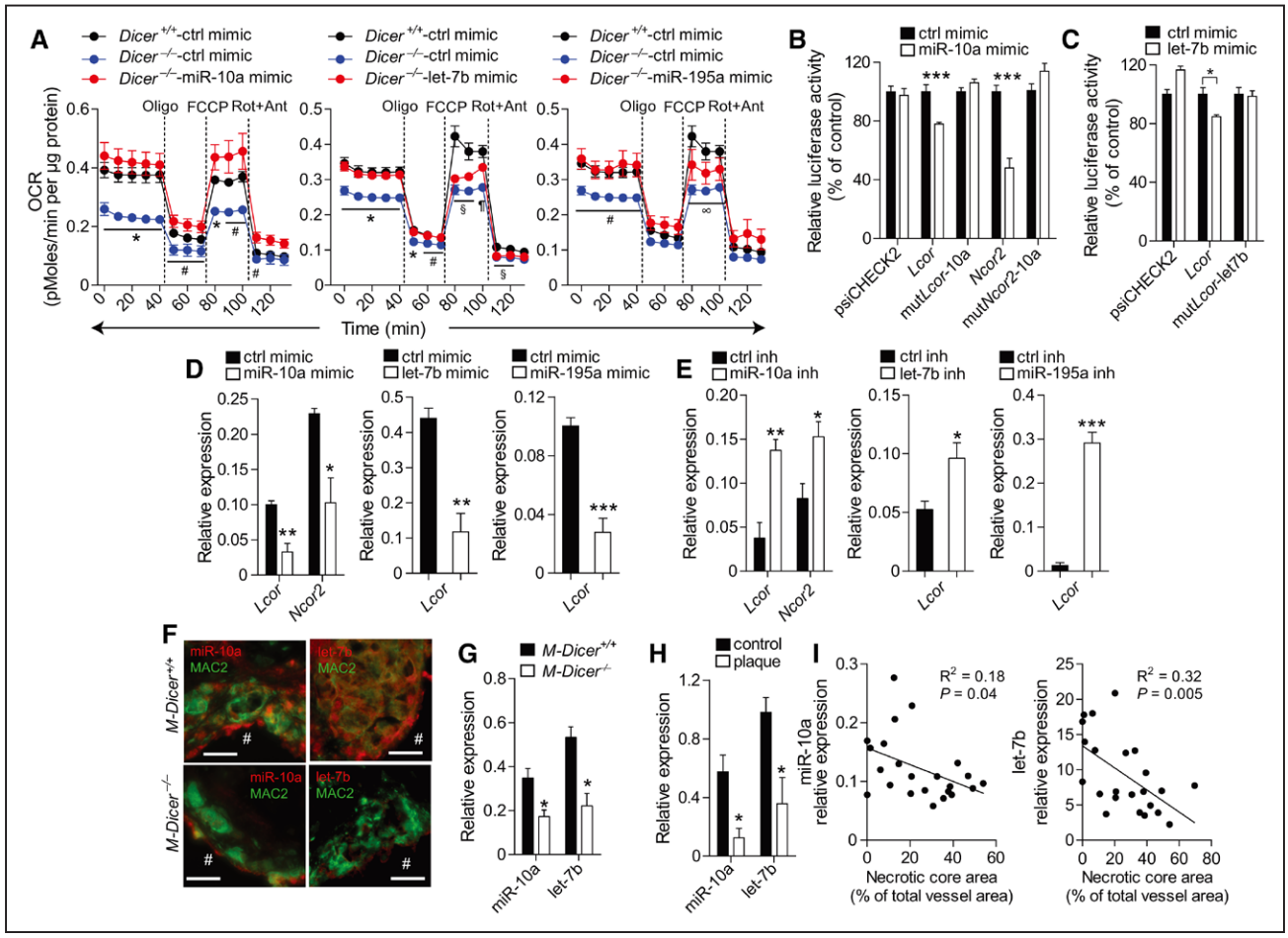

Figure 5. Ligand-dependent nuclear receptor corepressor (Lcor)–targeting microRNAs (miRNAs) miR-10a and let-7b contribute to the effect of Dicer in macrophages.

A, Oxygen consumption rate (OCR) of *Dicer*$^{-/-}$ and *Dicer*$^{+/+}$ alternatively activated macrophages (AAMs) transfected with miR-10a, let-7b, miR-195a or control (ctrl) mimics. n=3 or 4. **P*<0.05, blue vs red or black. #*P*<0.05, red vs blue. §*P*<0.05, black vs blue or red. ¶*P*<0.05 among all 3 groups. ∞*P*<0.05, black vs blue. **B** and **C**, Relative luciferase activity in HEK293T cells cotransfected with mimics of miR-10a (**B**) or let-7b (**C**) and the psiCHECK2 vectors containing *Lcor* 3′ untranslated region (UTR) without (*Lcor*) or with (mut*Lcor*-10a or mut*Lcor*-let7b) mutated binding site of miR-10a or let-7b or *Ncor2* 3′-UTR without (*Ncor2*) or with (mut*Ncor2*-10a) mutated binding site of miR-10a. n=5 or 6. **D** and **E**, Relative mRNA levels of *Ncor2* and/or *Lcor* in *Dicer*$^{-/-}$ AAMs transfected with miR-10a, let-7b, miR-195a, or control mimics (**D**; n=4 or 5) and in *Dicer*$^{+/+}$ AAMs transfected with miR-10a, let-7b, miR-195a, or control inhibitors (inh; **E**; n=3–5). **F**, Expression pattern of miR-10a and let-7b in aortic root lesions from *M-Dicer*$^{+/+}$ and *M-Dicer*$^{-/-}$ mice after 12-week high-fat diet (HFD) feeding period determined by combined in situ polymerase chain reaction and MAC2 immunostaining. #Lumen. Scale bars: 25 µm. **G** and **H**, Expression levels of miR-10a and let-7b in the aortas from *M-Dicer*$^{+/+}$ and *M-Dicer*$^{-/-}$ mice fed the HFD for 12 weeks (**G**) and in human vessel walls (control) and carotid plaques macroscopically dissected from the same atherosclerotic artery (**H**). n=3. **I**, Correlation of miR-10a and let-7b expression with necrotic core area in human carotid lesions. n=23. Data in **A** through **E**, **G**, and **H** are presented as mean±SEM. **P*<0.05, ***P*<0.005, and ****P*<0.001 by Student *t* test (**B** through **E**, **G**, and **H**) and 1-way ANOVA followed by Tukey-Kramer test (**A**). Oligo indicates oligomycin; and Rot+Ant, rotenone/antimycin.

miR-101, or miR-301 decreased the OCR in *Dicer*$^{-/-}$ BMDMs (Figure VI in the online-only Data Supplement). These findings suggest that Dicer promotes metabolic reprogramming of AAMs by generating miR-10a, let-7b, and miR-195a.

To determine the binding sites of these 3 miRNAs in the 3′-UTR of *Lcor*, we transfected HEK293T cells with a luciferase reporter vector containing the 3′-UTR of murine *Lcor*. Transfection of miR-10a and let-7b, but not of miR-195a, mimics reduced luciferase activities (Figure 5B and 5C and Figure VIIA in the online-only Data Supplement). Mutating the miR-10a and let-7b target site in *Lcor* 3′-UTR prevented the suppression of luciferase activities by miR-10a and let-7b mimics, respectively (Figure 5B and 5C and Figure VIIB in the online-only Data Supplement). In addition, we studied whether miR-10a targets the 3′-UTR of *Ncor2* (Figure VIIB in the online-only Data Supplement). Transfection of miR-10a mimics reduced luciferase activities in cells expressing the luciferase reporter gene fused to the wild-type 3′-UTR of *Ncor2* (Figure 5B). This effect was absent when the miR-10a target site in the *Ncor2* 3′-UTR was mutated (Figure 5B and Figure VIIB in the online-only Data Supplement). Gain-of-function and loss-of-function experiments showed that let-7b and miR-195a inhibit *Lcor* expression and that miR-10a suppresses *Lcor* and *Ncor2* expression in IL-4–treated BMDMs (Figure 5D and 5E).

We then studied the role of Dicer in the regulation of miR-10a and let-7b expression levels in lesional macrophages. In contrast to *M-Dicer*$^{+/+}$ mice, miR-10a and let-7b expression was reduced in lesional macrophages, as determined by combined in situ PCR and MAC2 immunostaining (Figure 5F) and in atherosclerotic aortas (Figure 5G) from *M-Dicer*$^{-/-}$ mice. In humans, miR-10a and let-7b expression levels were lower in carotid plaques than in the vessel wall (Figure 5H) and negatively correlated with the necrotic core area in carotid le-

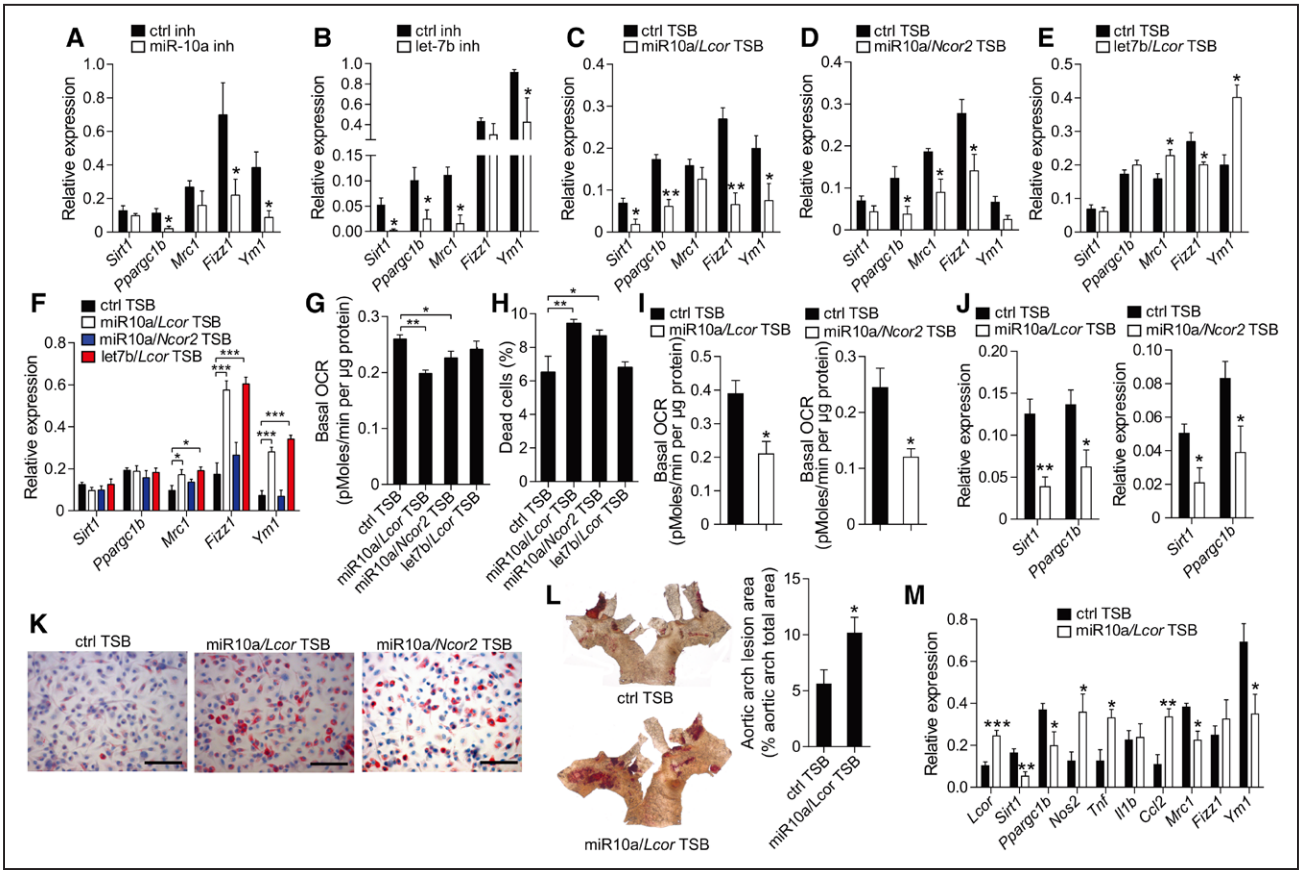

Figure 6. Effect of microRNA (miR)-10a on macrophages is mediated by targeting of ligand-dependent nuclear receptor corepressor (Lcor) and nuclear receptor corepressor 2 (Ncor2).

A through **E**, Relative mRNA levels of *Sirt1*, *Ppargc1b*, *Mrc1*, *Fizz1*, and *Ym1* in interleukin-4 (IL-4)–stimulated *M-Dicer*$^{+/+}$ bone marrow–derived macrophages (BMDMs) transfected with miR-10a inhibitor (inh; **A**), let-7b inhibitor (**B**), miR10a/*Lcor* target site blocker (TSB; **C**), miR10a/*Ncor2* TSB (**D**), let7b/*Lcor* TSB (**E**), or scrambled control (ctrl). n=3 to 5. **F**, Relative mRNA levels of *Sirt1*, *Ppargc1b*, *Mrc1*, *Fizz1*, and *Ym1* in IL-4–stimulated *Dicer*$^{+/+}$ BMDMs transfected with TSBs in the presence of CD3254. n=5 or 6. **G**, Basal oxygen consumption rate (OCR) of IL-4–treated *Dicer*$^{+/+}$ BMDMs transfected with TSBs. n=3 or 4. **H**, Cell death rate of IL-4–treated *Dicer*$^{+/+}$ BMDMs transfected with TSBs determined by flow cytometric analysis after Annexin V and propidium iodide staining. n=3 to 5. **I** through **K**, Basal OCR (**I**; n=3 or 4), relative mRNA levels of *Sirt1* and *Ppargc1b* (**J**; n=4 or 5), and Oil Red O staining (**K**; scale bars, 25 µm) in oxidized low-density lipoprotein (oxLDL)–treated *Dicer*$^{+/+}$ BMDMs transfected with miR10a/*Lcor*, miR10a/*Ncor2*, or control TSBs. **L** and **M**, Lesion formation in Oil Red O–stained, *en face*–prepared aortic arches (**L**; n=6 or 7) and relative expression of *Lcor*, *Sirt1*, *Ppargc1b*, inflammatory markers, and alternatively activated macrophage markers in thoracic aortas (**M**; n=5–7) from *Apoe*$^{-/-}$ mice treated with control or miR10a/*Lcor* TSBs during 12-week high-fat diet feeding program. All data except in **K** are presented as mean±SEM. **P*<0.05, ***P*<0.005, and ****P*<0.001 by Student *t* test (**A** through **E**, **I**, **J**, **L**, and **M**) and 1-way ANOVA followed by the Fisher least significant difference test (**F** through **H**).

sions (Figure 5I). These data suggest an atheroprotective role of miR-10a and let-7b expression in macrophages.

miR-10a Promotes Oxidative Metabolism by Targeting Lcor and Ncor2

Next, we studied the mechanisms by which miR-10a and let-7b affect metabolism during macrophage polarization. IL-4 and lipopolysaccharide/IFN-γ treatment upregulated and downregulated let-7b expression in BMDMs, respectively, but did not change miR-10a expression (Figure VIIC in the online-only Data Supplement). miR-10a inhibition reduced *Ppargc1b*, *Fizz1*, and *Ym1* expression (Figure 6A) and inhibition of let-7b downregulated *Sirt1*, *Ppargc1b*, *Mrc1*, and *Ym1* expression (Figure 6B) in IL-4–treated *Dicer*$^{+/+}$ BMDMs.

Locked nucleic acid–modified oligonucleotides and target site blockers (TSBs) were designed to block the interaction between miR-10a and *Lcor* (miR10a/*Lcor* TSBs) or *Ncor2* (miR10a/*Ncor2* TSBs) and between let-7b and *Lcor* (let7b/*Lcor* TSBs). We found that the TSBs specifically upregulated the expression of either *Lcor* or *Ncor2* in BMDMs (Figure VIID in the online-only Data Supplement). Transfection of miR10a/*Lcor* TSBs reduced the expression of *Sirt1*, *Ppargc1b*, *Fizz1*, and *Ym1* whereas transfection of miR10a/*Ncor2* TSBs reduced the expression of *Ppargc1b*, *Mrc1*, and *Fizz1* in IL–4-treated BMDMs (Figure 6C and 6D). Treatment with let7b/*Lcor* TSBs downregulated *Fizz1* and increased *Mrc1* and *Ym1* expression but did not alter *Sirt1* and *Ppargc1b* expression (Figure 6E). Treatment with CD3254 prevented miR10a/*Lcor* TSB-induced downregulation of *Sirt1* and *Ppargc1b* and miR10a/*Ncor2* TSB-induced downregulation of *Ppargc1b*, *Mrc1*, and *Fizz1* expression in IL-4–treated BMDMs (Figure 6F). Moreover, miR10a/*Lcor* TSBs or let7b/*Lcor* TSBs upregulated *Mrc1*, *Fizz1*, and *YM1* expression in BMDMs treated with CD3254 (Figure 6F).

In addition, transfection with miR10a/*Lcor* TSBs and, to a lesser extent, with miR10a/*Ncor2* TSBs, but not with let7b/*Lcor* TSBs, reduced the basal OCR (Figure 6G) and cell survival (Figure 6H) of IL-4–treated BMDMs. In oxLDL-treated BMDMs, transfection with miR10a/*Lcor* TSBs or miR10a/*Ncor2* TSBs decreased the basal OCR (Figure 6I), reduced *Sirt1* and *Ppargc1b* expression (Figure 6J), and enhanced lipid accumulation (Figure 6K). Taken together, these results suggest that miR-10a contributes to the effect of Dicer on mitochondrial respiration in AAMs and foam cells by targeting Lcor and Ncor2.

Therefore, we investigated the role of miR-10a–mediated suppression of Lcor in atherosclerosis. Treatment of *Apoe*$^{-/-}$ mice with miR10a/*Lcor* TSBs during the last 4 weeks of a 12-week HFD feeding program increased atherosclerotic lesion formation in the aortic arch compared with control TSBs (Figure 6L). Moreover, miR10a/*Lcor* TSB treatment reduced *Sirt1*, *Ppargc1b*, *Mrc1*, and *Ym1* expression and increased *Lcor*, *Nos2*, *Tnf*, and *Ccl2* expression in the aorta (Figure 6M). Injection of miR10a/*Lcor* TSBs increased the nuclear accumulation of LCoR in lesional macrophages (Figure VIIE in the online-only Data Supplement). The body weights, circulating leukocyte counts, and blood cholesterol levels did not differ between the groups (Table VII in the online-only Data Supplement). Hence, miR-10a may limit atherosclerotic lesion formation by suppressing *Lcor* in macrophages.

DISCUSSION

Our results show that miRNA biogenesis by Dicer plays a key role in the metabolic adaptation of macrophages to excessive fatty acid availability. Dicer increased mitochondrial FAO capacity in AAMs and foam cells by generating miRNAs such as miR-10a that promoted the expression of genes involved in mitochondrial oxidative metabolism by targeting Lcor. Dicer-mediated fatty acid degradation in macrophages reduced foam cell formation and lipotoxic stress and limited the progression of atherosclerosis to vulnerable lesions (Figure VIII in the online-only Data Supplement).

In contrast to storing fatty acids as triglycerides in lipid droplets in inflammatory macrophages, increased fatty acid availability through lysosomal lipolysis in AAMs results in enhanced OXPHOS and FAO,[22] which increases ATP production and enhances cell survival and phagocytosis.[22,27] Moreover, mitochondrial ATP production in AAMs is associated with decreased mitochondrial reactive oxygen species production and thus promotes an anti-inflammatory state.[18,41] We found that Dicer plays an essential role in the metabolic programming of IL-4–induced AAM polarization by enhancing mitochondrial biogenesis, OXPHOS, and ATP production. As a result, Dicer reduced inflammatory signaling and cytokine production in AAMs, similar to tumor-associated macrophages.[34] In vivo, myeloid cell–specific *Dicer* knockout induced a phenotypic shift of lesional macrophages toward a proinflammatory state, indicating that Dicer-mediated metabolic programming of AAMs limits the progression of atherosclerosis. Notably, increased oxygen consumption of macrophage-derived foam cells in early lesions ceases in advanced atherosclerosis.[5] Our findings reveal that excess lipid storage in foam cells triggers Dicer-mediated fatty acid degradation by mitochondrial respiration to reduce the triglyceride content in lipid droplets.[4] Thus, FAO and OXPHOS may protect lesional foam cells during early atherosclerosis from lipotoxicity as a result of the accumulation of triglycerides,[7] whereas the shutdown of mitochondrial respiration in lesional macrophages during inflammatory polarization may result in foam cell death and necrotic core

formation. Conversely, decreased fatty acid synthesis in macrophages limits triglyceride and cholesteryl ester accumulation and reduces foam cell formation in atherosclerosis.[42] Taken together, our findings indicate that Dicer expression in macrophages limits advanced atherosclerosis by increasing mitochondrial fatty acid degradation in foam cells. In contrast to its role in macrophages, endothelial Dicer promotes atherosclerosis by enhancing early monocyte recruitment.[43] Thus, the net effect of Dicer in the different cell types may depend heavily on the stage of atherosclerosis.

To investigate the mechanism by which Dicer promotes oxidative metabolism, we analyzed the miRNA targets in macrophages. We found that 2 nuclear receptor corepressors, Lcor and Ncor2, mediate the effect of *Dicer* knockout on mitochondrial respiration in AAMs. Notably, interaction with Ncor2 inhibits the activity of PPARs such as PPARα, which positively regulates the expression of *Ppargc1b*, *Sirt1*, and genes involved in FAO and OXPHOS,[44–46] and thereby reduces mitochondrial oxidative metabolism and increases the triglyceride content in adipocytes.[40] Hence, our results indicate a similar role of Ncor2 in mitochondrial function in AAMs. Moreover, Lcor attenuates agonist-activated nuclear receptor signaling, for example, the estrogen receptor-α and vitamin D receptor, by histone deacetylase–dependent and –independent mechanisms.[39] In addition, Lcor promotes Kruppel-like factor 6–mediated transcriptional repression of target genes.[47] We found that Lcor interacts with RXRα and inhibits RXR activity. RXRα acts as a sensor for mitochondrial function and upregulates mitochondrial genes by interacting with PGC-1.[48]

Among the miRNAs downregulated by *Dicer* knockout, miR-10a, let-7b, and miR-195a enhanced cellular oxygen consumption and suppressed Lcor expression, indicating that these 3 miRNAs contribute to the effect of Dicer in macrophages. In addition to target Ncor2, which is in line with previous reports,[49] miR-10a directly targets Lcor and thereby promotes mitochondrial function and an anti-inflammatory macrophage phenotype. Inhibition of this mechanism may play a key role in the proatherogenic and proinflammatory effect of TSBs that block the interaction between miR-10a and Lcor. Accordingly, miR-10a inhibits inflammatory monocyte activation by downregulating several components of the nuclear factor-κB pathway.[50] In contrast to miR-10a, the effect of let-7b on oxidative metabolism in macrophages was not meditated through targeting Lcor, indicating that other let-7b targets are involved in the regulation of macrophage metabolic reprogramming. Other let-7 family members such as let-7a, let-7i, and miR-98 did not affect metabolic reprogramming in AAMs, suggesting that the seed sequence is not essential for the let-7 effect in macrophages. Accordingly, the finding that let-7d partially mediates the effect of Dicer on polarization of tumor-associated macrophages may be the result of a different mechanism.[34] miR-195, the third miRNA that mediated the effect of Dicer on macrophage metabolism, suppressed Lcor not through direct targeting of its 3′-UTR. Hence, as-yet unknown miR-195 targets may promote Lcor expression and inhibit mitochondrial function.

CONCLUSIONS

Our findings demonstrate a critical role of Dicer in enhancing mitochondrial oxidative metabolism during alternative macrophage activation and foam cell formation by suppressing nuclear receptor corepressor Lcor through miR-10a, indicating that miRNAs coordinate the inflammatory response and lipid metabolism in macrophages by regulating mitochondrial function.

ARTICLE INFORMATION

Received September 8, 2017; accepted April 27, 2018.

The online-only Data Supplement is available with this article at https://www.ahajournals.org/doi/suppl/10.1161/circulationaha.117.031589.

Correspondence

Andreas Schober, MD, or Yuanyuan Wei, PhD, Experimental Vascular Medicine, Institute for Cardiovascular Prevention, Ludwig-Maximilians-University Munich, Pettenkoferstrasse 9b, 80336 Munich, Germany. E-mail aschober@med.lmu.de or yuanyuan.wei@med.uni-muenchen.de

Affiliations

Experimental Vascular Medicine, Institute for Cardiovascular Prevention (Y.W., J.C.-C., R.G., L.N., M.Z., C.G., A.S.), Biomedical Research Center, Biochemistry (N.E.), and Institut für Informatik (F.E., R.Z.), Ludwig-Maximilians-University Munich, Germany. DZHK (German Center for Cardiovascular Research), Partner Site Munich Heart Alliance, Germany (Y.W., A.S.). Helmholtz Diabetes Center and German Center for Diabetes Research, IDO, Munich, Germany (F.G., N.H.U.). Dr Erhard is currently at the Institut für Virologie, Julius-Maximilians-Universität Würzburg, Germany.

Acknowledgments

The authors thank J. Grommes (European Vascular Center Aachen-Maastricht, RWTH Aachen University) for providing the human carotid plaque samples. They also thank K. Heyll and L. Ruiz-Heinrich for technical assistance.

Sources of Funding

Dr Schober acknowledges support from the Deutsche Forschungsgemeinschaft (SFB 1123-B4), the DZHK (German Center for Cardiovascular Research) (MHA VD 1.2), and the German Federal Ministry of Education and Research (01KU1213A). Drs Schober and Wei acknowledge support from Else Kröner-Fresenius-Stiftung (2014_A219). Dr Wei acknowledges support from the DZHK (German Center for Cardiovascular Research) (FKZ 81X2600240) and the Deutsche Forschungsgemeinschaft (WE 6160/1–1). Drs Greulich and Unlenhaut acknowledge support from the Deutsche Forschungsgemeinschaft (UH275/1–1), and Dr Greulich acknowledges support from a Daimler Benz Scholarship. Drs Erhard and Zimmer acknowledge support from the Deutsche Forschungsgemeinschaft (SFB 1123-Z2).

Disclosures

None.

REFERENCES

1. Schober A, Weber C. Mechanisms of MicroRNAs in atherosclerosis. *Annu Rev Pathol*. 2016;11:583–616. doi: 10.1146/annurev-pathol-012615-044135
2. Tarbell JM. Mass transport in arteries and the localization of atherosclerosis. *Annu Rev Biomed Eng*. 2003;5:79–118. doi: 10.1146/annurev.bioeng.5.040202.121529
3. Canton J, Neculai D, Grinstein S. Scavenger receptors in homeostasis and immunity. *Nat Rev Immunol*. 2013;13:621–634. doi: 10.1038/nri3515
4. Malandrino MI, Fucho R, Weber M, Calderon-Dominguez M, Mir JF, Valcarcel L, Escoté X, Gómez-Serrano M, Peral B, Salvadó L, Fernández-Veledo S, Casals N, Vázquez-Carrera M, Villarroya F, Vendrell JJ, Serra D, Herrero L. Enhanced fatty acid oxidation in adipocytes and macrophages reduces lipid-induced triglyceride accumulation and inflammation. *Am J Physiol Endocrinol Metab*. 2015;308:E756–E769. doi: 10.1152/ajpendo.00362.2014
5. Björnheden T, Bondjers G. Oxygen consumption in aortic tissue from rabbits with diet-induced atherosclerosis. *Arteriosclerosis*. 1987;7:238–247.
6. Aon MA, Bhatt N, Cortassa SC. Mitochondrial and cellular mechanisms for managing lipid excess. *Front Physiol*. 2014;5:282. doi: 10.3389/fphys.2014.00282
7. Aflaki E, Radovic B, Chandak PG, Kolb D, Eisenberg T, Ring J, Fertschai I, Uellen A, Wolinski H, Kohlwein SD, Zechner R, Levak-Frank S, Sattler W, Graier WF, Malli R, Madeo F, Kratky D. Triacylglycerol accumulation activates the mitochondrial apoptosis pathway in macrophages. *J Biol Chem*. 2011;286:7418–7428. doi: 10.1074/jbc.M110.175703
8. Henson PM. Cell removal: efferocytosis. *Annu Rev Cell Dev Biol*. 2017;33:127–144. doi: 10.1146/annurev-cellbio-111315-125315
9. Hamon Y, Broccardo C, Chambenoit O, Luciani MF, Toti F, Chaslin S, Freyssinet JM, Devaux PF, McNeish J, Marguet D, Chimini G. ABC1 promotes engulfment of apoptotic cells and transbilayer redistribution of phosphatidylserine. *Nat Cell Biol*. 2000;2:399–406. doi: 10.1038/35017029
10. Röszer T. Transcriptional control of apoptotic cell clearance by macrophage nuclear receptors. *Apoptosis*. 2017;22:284–294. doi: 10.1007/s10495-016-1310-x
11. Yvan-Charvet L, Pagler TA, Seimon TA, Thorp E, Welch CL, Witztum JL, Tabas I, Tall AR. ABCA1 and ABCG1 protect against oxidative stress-induced macrophage apoptosis during efferocytosis. *Circ Res*. 2010;106:1861–1869. doi: 10.1161/CIRCRESAHA.110.217281
12. Tabas I, Bornfeldt KE. Macrophage phenotype and function in different stages of atherosclerosis. *Circ Res*. 2016;118:653–667. doi: 10.1161/CIRCRESAHA.115.306256
13. Narula J, Nakano M, Virmani R, Kolodgie FD, Petersen R, Newcomb R, Malik S, Fuster V, Finn AV. Histopathologic characteristics of atherosclerotic coronary disease and implications of the findings for the invasive and noninvasive detection of vulnerable plaques. *J Am Coll Cardiol*. 2013;61:1041–1051. doi: 10.1016/j.jacc.2012.10.054
14. Feingold KR, Shigenaga JK, Kazemi MR, McDonald CM, Patzek SM, Cross AS, Moser A, Grunfeld C. Mechanisms of triglyceride accumulation in activated macrophages. *J Leukoc Biol*. 2012;92:829–839. doi: 10.1189/jlb.1111537
15. Huang YL, Morales-Rosado J, Ray J, Myers TG, Kho T, Lu M, Munford RS. Toll-like receptor agonists promote prolonged triglyceride storage in macrophages. *J Biol Chem*. 2014;289:3001–3012. doi: 10.1074/jbc.M113.524587
16. Pearce EL, Pearce EJ. Metabolic pathways in immune cell activation and quiescence. *Immunity*. 2013;38:633–643. doi: 10.1016/j.immuni.2013.04.005
17. West AP, Brodsky IE, Rahner C, Woo DK, Erdjument-Bromage H, Tempst P, Walsh MC, Choi Y, Shadel GS, Ghosh S. TLR signalling augments macrophage bactericidal activity through mitochondrial ROS. *Nature*. 2011;472:476–480. doi: 10.1038/nature09973
18. Mills EL, Kelly B, Logan A, Costa ASH, Varma M, Bryant CE, Tourlomousis P, Däbritz JHM, Gottlieb E, Latorre I, Corr SC, McManus G, Ryan D, Jacobs HT, Szibor M, Xavier RJ, Braun T, Frezza C, Murphy MP, O'Neill LA. Succinate dehydrogenase supports metabolic repurposing of mitochondria to drive inflammatory macrophages. *Cell*. 2016;167:457–470.e13. doi: 10.1016/j.cell.2016.08.064
19. Takeda N, O'Dea EL, Doedens A, Kim JW, Weidemann A, Stockmann C, Asagiri M, Simon MC, Hoffmann A, Johnson RS. Differential activation and antagonistic function of HIF-{alpha} isoforms in macrophages are essential for NO homeostasis. *Genes Dev*. 2010;24:491–501. doi: 10.1101/gad.1881410
20. Kelly B, O'Neill LA. Metabolic reprogramming in macrophages and dendritic cells in innate immunity. *Cell Res*. 2015;25:771–784. doi: 10.1038/cr.2015.68
21. Everts B, Amiel E, van der Windt GJ, Freitas TC, Chott R, Yarasheski KE, Pearce EL, Pearce EJ. Commitment to glycolysis sustains survival of NO-producing inflammatory dendritic cells. *Blood*. 2012;120:1422–1431. doi: 10.1182/blood-2012-03-419747
22. Huang SC, Everts B, Ivanova Y, O'Sullivan D, Nascimento M, Smith AM, Beatty W, Love-Gregory L, Lam WY, O'Neill CM, Yan C, Du H, Abumrad NA, Urban JF Jr, Artyomov MN, Pearce EL, Pearce EJ. Cell-intrinsic lysosomal lipolysis is essential for alternative activation of macrophages. *Nat Immunol*. 2014;15:846–855. doi: 10.1038/ni.2956
23. Vats D, Mukundan L, Odegaard JI, Zhang L, Smith KL, Morel CR, Wagner RA, Greaves DR, Murray PJ, Chawla A. Oxidative metabolism and PGC-1beta attenuate macrophage-mediated inflammation. *Cell Metab*. 2006;4:13–24. doi: 10.1016/j.cmet.2006.05.011
24. St-Pierre J, Lin J, Krauss S, Tarr PT, Yang R, Newgard CB, Spiegelman BM. Bioenergetic analysis of peroxisome proliferator-activated receptor gamma coactivators 1alpha and 1beta (PGC-1alpha and PGC-1beta) in muscle cells. *J Biol Chem*. 2003;278:26597–26603. doi: 10.1074/jbc.M301850200
25. Liu TF, Vachharajani VT, Yoza BK, McCall CE. NAD+-dependent sirtuin 1 and 6 proteins coordinate a switch from glucose to fatty acid oxidation during the acute inflammatory response. *J Biol Chem*. 2012;287:25758–25769. doi: 10.1074/jbc.M112.362343
26. Kelly TJ, Lerin C, Haas W, Gygi SP, Puigserver P. GCN5-mediated transcriptional control of the metabolic coactivator PGC-1beta through lysine acetylation. *J Biol Chem*. 2009;284:19945–19952. doi: 10.1074/jbc.M109.015164
27. Chandak PG, Radovic B, Aflaki E, Kolb D, Buchebner M, Fröhlich E, Magnes C, Sinner F, Haemmerle G, Zechner R, Tabas I, Levak-Frank S, Kratky D. Efficient phagocytosis requires triacylglycerol hydrolysis by adipose triglyceride lipase. *J Biol Chem*. 2010;285:20192–20201. doi: 10.1074/jbc.M110.107854
28. Wei Y, Schober A. MicroRNA regulation of macrophages in human pathologies. *Cell Mol Life Sci*. 2016;73:3473–3495. doi: 10.1007/s00018-016-2254-6
29. Wei Y, Nazari-Jahantigh M, Chan L, Zhu M, Heyll K, Corbalán-Campos J, Hartmann P, Thiemann A, Weber C, Schober A. The microRNA-342-5p fosters inflammatory macrophage activation through an Akt1- and microRNA-155-dependent pathway during atherosclerosis. *Circulation*. 2013;127:1609–1619. doi: 10.1161/CIRCULATIONAHA.112.000736
30. Wei Y, Zhu M, Corbalán-Campos J, Heyll K, Weber C, Schober A. Regulation of Csf1r and Bcl6 in macrophages mediates the stage-specific effects of microRNA-155 on atherosclerosis. *Arterioscler Thromb Vasc Biol*. 2015;35:796–803. doi: 10.1161/ATVBAHA.114.304723
31. Ha M, Kim VN. Regulation of microRNA biogenesis. *Nat Rev Mol Cell Biol*. 2014;15:509–524. doi: 10.1038/nrm3838
32. Helwak A, Kudla G, Dudnakova T, Tollervey D. Mapping the human miRNA interactome by CLASH reveals frequent noncanonical binding. *Cell*. 2013;153:654–665. doi: 10.1016/j.cell.2013.03.043
33. Gross TJ, Powers LS, Boudreau RL, Brink B, Reisetter A, Goel K, Gerke AK, Hassan IH, Monick MM. A microRNA processing defect in smokers' macrophages is linked to SUMOylation of the endonuclease DICER. *J Biol Chem*. 2014;289:12823–12834. doi: 10.1074/jbc.M114.565473
34. Baer C, Squadrito ML, Laoui D, Thompson D, Hansen SK, Kiialainen A, Hoves S, Ries CH, Ooi CH, De Palma M. Suppression of microRNA activity amplifies IFN-γ-induced macrophage activation and promotes anti-tumour immunity. *Nat Cell Biol*. 2016;18:790–802. doi: 10.1038/ncb3371
35. Harfe BD, McManus MT, Mansfield JH, Hornstein E, Tabin CJ. The RNaseIII enzyme Dicer is required for morphogenesis but not patterning of the vertebrate limb. *Proc Natl Acad Sci USA*. 2005;102:10898–10903. doi: 10.1073/pnas.0504834102
36. Erhard F, Dölken L, Zimmer R. RIP-chip enrichment analysis. *Bioinformatics*. 2013;29:77–83. doi: 10.1093/bioinformatics/bts631
37. Dobin A, Davis CA, Schlesinger F, Drenkow J, Zaleski C, Jha S, Batut P, Chaisson M, Gingeras TR. STAR: ultrafast universal RNA-seq aligner. *Bioinformatics*. 2013;29:15–21. doi: 10.1093/bioinformatics/bts635
38. Love MI, Huber W, Anders S. Moderated estimation of fold change and dispersion for RNA-seq data with DESeq2. *Genome Biol*. 2014;15:550. doi: 10.1186/s13059-014-0550-8
39. Fernandes I, Bastien Y, Wai T, Nygard K, Lin R, Cormier O, Lee HS, Eng F, Bertos NR, Pelletier N, Mader S, Han VK, Yang XJ, White JH. Ligand-dependent nuclear receptor corepressor lcor functions by histone deacetylase-dependent and -independent mechanisms. *Mol. Cell*. 2003;11:139–150. doi: 10.1016/S1097-2765(03)00014-5

40. Reilly SM, Bhargava P, Liu S, Gangl MR, Gorgun C, Nofsinger RR, Evans RM, Qi L, Hu FB, Lee CH. Nuclear receptor corepressor SMRT regulates mitochondrial oxidative metabolism and mediates aging-related metabolic deterioration. *Cell Metab*. 2010;12:643–653. doi: 10.1016/j.cmet.2010.11.007
41. Mills EL, Kelly B, O'Neill LAJ. Mitochondria are the powerhouses of immunity. *Nat Immunol*. 2017;18:488–498. doi: 10.1038/ni.3704
42. Schneider JG, Yang Z, Chakravarthy MV, Lodhi IJ, Wei X, Turk J, Semenkovich CF. Macrophage fatty-acid synthase deficiency decreases diet-induced atherosclerosis. *J Biol Chem*. 2010;285:23398–23409. doi: 10.1074/jbc.M110.100321
43. Hartmann P, Zhou Z, Natarelli L, Wei Y, Nazari-Jahantigh M, Zhu M, Grommes J, Steffens S, Weber C, Schober A. Endothelial Dicer promotes atherosclerosis and vascular inflammation by miRNA-103-mediated suppression of KLF4. *Nat Commun*. 2016;7:10521. doi: 10.1038/ncomms10521
44. Feingold KR, Wang Y, Moser A, Shigenaga JK, Grunfeld C. LPS decreases fatty acid oxidation and nuclear hormone receptors in the kidney. *J Lipid Res*. 2008;49:2179–2187. doi: 10.1194/jlr.M800233-JLR200
45. Hayashida S, Arimoto A, Kuramoto Y, Kozako T, Honda S, Shimeno H, Soeda S. Fasting promotes the expression of SIRT1, an NAD+ -dependent protein deacetylase, via activation of PPARalpha in mice. *Mol Cell Biochem*. 2010;339:285–292. doi: 10.1007/s11010-010-0391-z
46. Kersten S. Integrated physiology and systems biology of PPARα. *Mol Metab*. 2014;3:354–371. doi: 10.1016/j.molmet.2014.02.002
47. Calderon MR, Verway M, An BS, DiFeo A, Bismar TA, Ann DK, Martignetti JA, Shalom-Barak T, White JH. Ligand-dependent corepressor (LCoR) recruitment by Kruppel-like factor 6 (KLF6) regulates expression of the cyclin-dependent kinase inhibitor CDKN1A gene. *J Biol Chem*. 2012;287:8662–8674. doi: 10.1074/jbc.M111.311605
48. Chae S, Ahn BY, Byun K, Cho YM, Yu MH, Lee B, Hwang D, Park KS. A systems approach for decoding mitochondrial retrograde signaling pathways. *Sci Signal*. 2013;6:rs4. doi: 10.1126/scisignal.2003266
49. Foley NH, Bray I, Watters KM, Das S, Bryan K, Bernas T, Prehn JH, Stallings RL. MicroRNAs 10a and 10b are potent inducers of neuroblastoma cell differentiation through targeting of nuclear receptor corepressor 2. *Cell Death Differ*. 2011;18:1089–1098. doi: 10.1038/cdd.2010.172
50. Njock MS, Cheng HS, Dang LT, Nazari-Jahantigh M, Lau AC, Boudreau E, Roufaiel M, Cybulsky MI, Schober A, Fish JE. Endothelial cells suppress monocyte activation through secretion of extracellular vesicles containing antiinflammatory microRNAs. *Blood*. 2015;125:3202–3212. doi: 10.1182/blood-2014-11-611046